Received: 11.02.2026 | Revision: 20.02.2026 | Accepted: 20.02.2026 | Published: 25.06.2026

Veterinary Sciences

doi: 10.31210/spi2026.29.01.38
UDC 579.84:604.2:620.3]:615.281

ORIGINAL ARTICLE

Scientific Progress & Innovations
ISSN: 2786-8842 (Print)
2786-8850 (Online)

29 (1)
2026

Green synthesis of Iron nanoparticles from *Pseudomonas aeruginosa* isolated from soil and their antibacterial and antibiofilm activity against pathogenic bacteria

I. J. Abbass[1] | E. A. Al-Imara[2] | D. A. Alhasan[3]

Article info

Correspondence Author
I. J. Abbass
E-mail:
ismail.abbs@uobasrah.edu.iq

[1] College of Education, Quran, University of Basrah, University of Basrah, Basrah, 61016 Iraq

[2] Marine Science Center, University of Basrah, Basrah, 61001 Iraq

[3] College of Veterinary Medicine, University of Shatrah, Nasiriyah, 64001 Iraq

Citation: Abbass, I. J., Al-Imara, E. A., & Alhasan, D. A. (2026). Green synthesis of iron nanoparticles from *Pseudomonas aeruginosa* isolated from soil and their antibacterial and antibiofilm activity against pathogenic bacteria. *Scientific Progress & Innovations*, 29(1), 244–254. doi: 10.31210/spi2026.29.01.38

Fifty-four soil samples were collected from various sites (agricultural, oil-polluted, riverbank, and animal dung-contaminated soils) in northern Basrah, southern Iraq, between September 18 and November 28, 2022. The specimens were transported to the laboratory within 3 hours, serially diluted, and cultivated on selective media. The screening indicated that 28 samples (51.9 %) exhibited positive bacterial growth. Phenotypic and molecular identification via PCR amplification of the 16S rRNA gene (~1400 bp) revealed the presence of *Pseudomonas aeruginosa* (8 isolates), *Escherichia coli* (7 isolates), *Klebsiella pneumoniae* (4 isolates), *Staphylococcus aureus* (4 isolates), *Bacillus cereus* (3 isolates), and *Bacillus subtilis* (2 isolates). Among these, a dominant *P. aeruginosa* isolate was successfully utilized for the green biosynthesis of iron nanoparticles (FeNPs). The successful formation of biogenic FeNPs was initially indicated by a rapid color transition from yellow to dark brown. UV-Vis spectroscopy confirmed nanoparticle synthesis with a sharp surface plasmon resonance peak at 304 nm, while FT-IR spectroscopy verified the definitive metal-oxygen (Fe–O) stretching bond at 589.97 cm^{-1} along with capping bacterial functional groups. Scanning electron microscopy (SEM) demonstrated a predominantly spherical nanoparticle morphology with a well-defined representative particle size of 22.83 nm. The quantitative microtiter plate and Congo red agar assays confirmed that the pathogenic isolates possessed a robust baseline capacity for biofilm formation. The biosynthesized FeNPs exhibited exceptional, concentration-dependent antibiofilm efficacy, achieving characteristically high biofilm inhibition rates of up to 91.64 % at concentrations of 50 and 100 µg/mL. Furthermore, the nanoparticles displayed potent antibacterial activity via the agar well diffusion method, with inhibition zones expanding proportionally with concentration and reaching a maximum diameter of 21.0 mm against *P. aeruginosa*. These collective findings suggest that biosynthesized iron nanoparticles could serve as highly effective, biocompatible, and environmentally friendly nano-antimicrobials for mitigating multidrug-resistant pathogens and persistent biofilm-associated infections.

Keywords: *Pseudomonas aeruginosa*, Iron nanoparticles, Green synthesis, antibiofilm, antibacterial activity.

Зелений синтез наночастинок заліза за допомогою *Pseudomonas aeruginosa*, виділеної з ґрунту, та їхня антибактеріальна й антибіоплівкова активність проти патогенних бактерій

І. Дж. Аббасс[1] | Е. А. Аль-Імара[2] | Д. А. Альхасан[3]

[1] Педагогічний факультет в Ель-Курні, Університет Басри, Басра, Ірак

[2] Центр морських наук, Університет Басри, Басра, Ірак

[3] Факультет ветеринарної медицини, Університет Шатри, Насирія, Ірак

У період з 18 вересня по 28 листопада 2022 року з різних локацій у північній частині Басри (південний Ірак) було відібрано 54 зразки ґрунту (сільськогосподарські, забруднені нафтою, прибережні ґрунти, а також ґрунти, забруднені тваринним гноєм). Зразки транспортували до лабораторії протягом 3 годин, після чого виконували серійні розведення та висів на селективні живильні середовища. Первинний скринінг показав, що 28 зразків (51,9 %) продемонстрували позитивний ріст бактерій. За допомогою фенотипової та молекулярно-генетичної ідентифікації шляхом ПЛР-ампліфікації гена 16S рРНК (~1400 пар основ) було підтверджено наявність таких видів бактерій: *Pseudomonas aeruginosa* (8 ізолятів), *Escherichia coli* (7 ізолятів), *Klebsiella pneumoniae* (4 ізоляти), *Staphylococcus aureus* (4 ізоляти), *Bacillus cereus* (3 ізоляти) та *Bacillus subtilis* (2 ізоляти). Серед них найбільш поширений ізолят *P. aeruginosa* було успішно використано для зеленого біосинтезу наночастинок заліза (FeNPs). На початковому етапі формування біогенних FeNPs спостерігалася швидка зміна кольору реакційної суміші з жовтого на темно-коричневий. Метод УФ-видимої спектроскопії підтвердив синтез наночастинок за наявністю чіткого піку поверхневого плазмонного резонансу при 304 нм, тоді як ІЧ-спектроскопія з перетворенням Фур'є остаточно верифікувала формування характерного валентного зв'язку метал-кисень (Fe–O) при 589,97 $см^{-1}$ разом із функціональними групами бактеріальних біомолекул оболонки. Скануюча електронна мікроскопія продемонструвала переважно сферичну морфологію наночастинок із чітко визначеним репрезентативним розміром 22,83 нм. Кількісний аналіз у мікротитрованих планшетах та тест на агарі з конго червоним підтвердили, що досліджувані патогенні ізоляти мали високу базову здатність до формування біоплівок. Біосинтезовані FeNPs виявили виняткову дозозалежну антибіоплівкову ефективність, забезпечуючи високі показники пригнічення біоплівок – до 91,64 % при концентраціях 50 і 100 мкг/мл. Крім того, наночастинки продемонстрували потужну антибактеріальну дію за методом дифузії в агар: зони пригнічення росту збільшувалися пропорційно до концентрації, досягаючи максимального діаметра 21,0 мм відносно *P. aeruginosa*. У сукупності ці результати свідчать про те, що біосинтезовані наночастинки заліза можуть слугувати високоефективною, біосумісною та екологічно безпечною альтернативою антибіотикам для боротьби з мультирезистентними патогенами та хронічними інфекціями, асоційованими з біоплівками.

Ключові слова: *Pseudomonas aeruginosa*, наночастинки заліза, зелений синтез, антибіоплівкова дія, антибактеріальна активність.

OPEN ACCESS

Бібліографічний опис для цитування: *Аббасс І. Дж., Аль-Імара Е. А., Альхасан Д. А.* Зелений синтез наночастинок заліза за допомогою Pseudomonas aeruginosa, виділеної з ґрунту, та їхня антибактеріальна й антибіоплівкова активність проти патогенних бактерій. *Scientific Progress & Innovations*. 2026. № 29 (1). С. 244–254.

Introduction

Pseudomonas aeruginosa is a Gram-negative, asporogenous, and monoflagellated bacterium [1]. It is a highly versatile and adaptable bacterial species prevalent in the environment, possessing a wide variety of virulence genes, substantial clinical significance, and numerous innate or acquired antibiotic resistance traits. Additionally, *P. aeruginosa* expresses multiple intrinsic and acquired antimicrobial resistance (AMR) mechanisms, including low outer-membrane permeability, expression of efflux pumps, and chromosomal or plasmid-mediated β-lactamases. Due to limited treatment options, its association with increased mortality, and longer ICU stays, *P. aeruginosa* is currently classified by the World Health Organization as a critical-priority pathogen [2].

Biofilm-embedded cells of this pathogen are highly tolerant to antibiotics, disinfectants, and host immunity. This tolerance predisposes patients to chronic colonization, graft failure, and progression to sepsis [2]. Consequently, interest in developing various nanomaterials via green chemistry to control microbial pathogens has grown significantly, driven by the numerous benefits of nanotechnology [3]. Furthermore, these nanomaterials have found widespread use in a variety of applications, including antioxidants, nanosensors, anticancer agents, and coatings for medical devices [4].

For the synthesis of nanoparticles (NPs), employing green chemistry instead of conventional physical and chemical methods offers several distinct advantages, including greater cost-effectiveness, simplicity, reduced environmental impact, and lower release of hazardous chemicals [3]. Nanoparticles possess unique properties that make them a promising approach for treating microbial infections, such as small size, large surface area-to-volume ratio, high stability, biocompatibility, targeted delivery capabilities, and enhanced cellular interactions. In recent years, green chemistry has facilitated the synthesis of biocompatible NPs effective in controlling biofilm-related infections while minimizing the reliance on conventional antibiotics. Several studies have reported the potential of green-synthesized nanoparticles to combat biofilms formed by both mono- and polymicrobial pathogens associated with severe diseases. Various biological sources – such as plants, animals, microorganisms, and algae – have been widely utilized in NP synthesis, where their biomolecules play a crucial role as reducing and stabilizing agents during nanoparticle formation [5].

These NPs have been synthesized using a wide variety of biological materials, including plants, animals, bacteria, and algae. The production process involves several biomolecules from these biological sources; these molecules form a corona around the nanoparticles, enhancing their stability and biocompatibility [3]. Furthermore, by interacting with the cell membrane and undergoing internalization, the corona layer covering the NPs increases their biological efficacy. When this corona is derived from microbial species, it can facilitate contact with the cell surface of microbial pathogens that share similar structural components, thereby helping to inhibit biofilm-forming microbes [6].

One of the most critical elements required by these bacteria is iron. The fact that iron-dependent genes account for approximately 6 % of overall gene expression underscores the vital importance of this element. In *P. aeruginosa*, fluctuations in iron levels influence intracellular signaling and subsequent biofilm development. These mechanisms demonstrate how crucial iron is to the lifecycle of this opportunistic pathogen [7].

The current study aims to apply this concept by synthesizing bacterial-inspired nanoparticles designed to suppress biofilm formation and reduce the virulence of bacterial pathogens. Specifically, utilizing *P. aeruginosa* siderophores as a surface corona in nanoparticle synthesis represents a promising strategy for developing potential antivirulence and antibiofilm agents. Nanoparticles synthesized using siderophores may be recognized by specific bacterial receptor proteins and active transport systems. Because these cellular systems naturally identify siderophore molecules, they can facilitate nanoparticle entry into bacterial cells, subsequently leading to cell death.

The aim of the study

Therefore, this study aimed to isolate bacterial species from various soil samples, identify the most prevalent species, utilize them for the biosynthesis of iron nanoparticles, and evaluate their resulting antimicrobial and antibiofilm activities.

Materials and methods

Samples collection

A total of fifty-four soil samples were collected from various sites in northern Basrah, southern Iraq, specifically from the Al-Qurna and Al-Madinah districts. The samples represented diverse environments, including agricultural soil, oil-polluted areas, riverbanks (Tigris and Euphrates), sewage-impacted sites, and soil contaminated with animal dung. The samples were obtained under sterile conditions by digging 5 cm into the ground using a shovel and were collected in sterilized plastic bottles. All samples were labeled with relevant metadata (location, date, and soil type) and transferred to the laboratory within 3 hours. For processing, 1 gram of each soil sample was suspended in a test tube containing 10 mL of distilled water. Serial tenfold dilutions ranging from 10^{-1} to 10^{-5} CFU/mL were prepared using a micropipette. Subsequently, a 0.5 mL aliquot from the dilutions was inoculated onto nutrient agar plates and incubated overnight at 37 °C [8].

Isolation of bacteria

Bacterial isolation was performed by cultivating the samples on different selective and differential culture media, including nutrient agar, blood agar, and MacConkey agar.

Bacterial identification

Microscopic identification

The isolated bacteria were subjected to Gram staining and examined under an optical microscope to evaluate

their Gram reaction (Gram-positive or Gram-negative) and cellular morphology.

Phenotypic identification

Bacterial isolates grown on the various media were phenotypically identified based on macro-morphological characteristics of the colonies, including color, margin shape, elevation, and size.

Genetic identification

For *Pseudomonas aeruginosa* isolates selected for the biosynthesis of iron nanoparticles (FeNPs), genomic DNA was extracted using the Presto™ Mini gDNA Bacteria Kit (Geneaid) following the manufacturer's protocol. The quality and concentration of the extracted DNA were evaluated via agarose gel electrophoresis according to the method described by [9]. The purified genomic DNA then served as a template for PCR amplification using Primax PCR Master Mix. The 16S rRNA gene was amplified using specific primers according to the protocol described by [10], targeting an expected amplicon size of 1400 bp. The primer sequences utilized were:

- F: 5′-AGAGTTTGATCMTGGCTCAG-3′
- R: 5′-TACGGTACCTTGTTACGACTT-3′

Detection of biofilm-forming bacterial isolates

Congo red agar method

The screening for biofilm-forming isolates was conducted using the Congo red agar medium, following the procedure described by [11].

Microtiter plate (MTP) assay

Biofilm formation by the bacterial isolates was quantified using the microtiter plate method according to the protocol by [12]. The optical density (OD) of each well was measured using a Multiskan Go spectrophotometer at a wavelength of 630 nm according to [13]. Biofilm formation capacity was determined using the following parameters:

- A: Absorbance of the test wells containing the bacterial suspension with the culture medium.
- A_C: Absorbance of the control wells containing only the culture medium.

The strength of biofilm formation was categorized as follows:

- $A \leq A_C$: Non-biofilm producer (Negative)
- $A_C < A \leq 2 \times A_C$: Moderate biofilm producer
- $A > 2 \times A_C$: Strong/High biofilm producer

Synthesis of extracellular iron nanoparticles (FeNPs) from P. aeruginosa

Preparation of P. aeruginosa supernatant

The selected *P. aeruginosa* isolate was inoculated into nutrient broth and incubated in a shaking incubator at 150 rpm and 37 °C for 48 hours to generate sufficient biomass. Afterward, the culture was centrifuged at 6,000 rpm to pellet the bacterial cells. The cell-free supernatant was collected and stored at 4 °C until further use.

Biosynthesis of iron nanoparticles (FeNPs)

To prepare the precursor solution, 0.5 g of iron nitrate [$Fe(NO_3)_3 \cdot 9H_2O$] was dissolved in 100 mL of sterile distilled water to achieve a final concentration of 0.01 mM and stored until use. Subsequently, 100 mL of this iron nitrate solution was mixed with 100 mL of the *P. aeruginosa* cell-free supernatant. A rapid change in the color of the mixture indicated the initial formation of nanoparticles.

Purification of nanoparticles

The synthesized nanoparticles were harvested by centrifugation at 6,000 rpm for 15 minutes to collect the pellet and remove the supernatant. The resulting precipitate was washed three times with double-distilled water (DDW). Finally, the purified nanoparticles were dried in a hot air oven at 100 °C for 3 hours, yielding dry FeNPs ready for subsequent characterization assays.

Characterization of FeNPs

Visual observation (color change)

The initial indication of the successful biosynthesis of iron nanoparticles was monitored via the visual color change of the reaction solution.

UV-visible spectroscopy

1. A 3 mL aliquot of the initial *P. aeruginosa* cell-free supernatant was analyzed in the spectrophotometer to establish the baseline absorbance.

2. Subsequently, a 3 mL aliquot of the reaction mixture was collected after the color change, and its absorbance spectrum was recorded. The resulting profiles were compared against the baseline supernatant spectrum to confirm nanoparticle synthesis.

FT-IR spectroscopy

A FT-IR 4600 spectrometer was used to identify the functional groups present in the bacterial supernatant solution that are responsible for the reduction of mineral salts. The spectra were recorded with a resolution of 4 cm^{-1}. For analysis, 0.1 mg of the synthesized nanomaterial was weighed and dissolved in 10 mL of dimethyl sulfoxide (DMSO). The mixture was then placed in an ultrasonic bath for 16 minutes to ensure complete homogenization of the material within the solvent. Subsequently, a 5–10 µL aliquot was pipetted and placed onto the crystal lens. After ensuring the complete absence of air bubbles, the sample was secured using the pressure arm, and the measurement was conducted [14].

Scanning electron microscopy (SEM)

The morphological properties of the nanoparticles were analyzed using scanning electron microscopy (SEM) for surface imaging. This method reveals the shape, structural characteristics, and size distribution of the nanoparticles. It also provides essential information regarding the level of agglomeration, particle aggregation, and purity of the synthesized material. Modern SEM instruments are capable of determining the morphology of nanoparticles smaller than 15 nm. For characterization, approximately 0.5 g of the dry nanomaterial was weighed and submitted to the central SEM laboratory for analysis [15].

Evaluation of the antibiofilm activity of FeNPs

The microtiter plate assay, as described by [16], was used to evaluate the antibiofilm activity of the synthesized iron nanoparticles (FeNPs). Biofilm-forming bacterial isolates were initially activated on nutrient agar. A 5 mL aliquot of Brain Heart Infusion (BHI) broth supplemented with 2 % glucose was prepared in sterile test tubes, and the bacterial cultures were inoculated into the medium. Subsequently, 100 µL of the resulting bacterial suspension was distributed into individual wells of a sterile 96-well microtiter plate.

For each isolate, wells containing the bacterial suspension without nanoparticles served as the negative control. Iron nanoparticles were added to the remaining wells at concentrations ranging from 50 to 100 µg/mL in a horizontal arrangement, with three replicates for each concentration. The plates were then incubated at 37 °C for 24 hours to allow biofilm development.

Following the incubation period, the contents of the wells were carefully aspirated, and each well was washed three times with phosphate-buffered saline (PBS) to eliminate non-adherent cells. The adhered biofilms were stained with a 3 % crystal violet solution and incubated at room temperature for 15 minutes. Subsequently, 100 µL of 93 % methanol was added to each well for 10 minutes to fix the attached cells. Following fixation, the wells were emptied and washed three times with distilled water to remove excess stain. To solubilize the bound dye, 160 µL of 33 % glacial acetic acid was added to each well. The optical density (OD) was then measured at 630 nm using a Multiskan™ Go microplate reader. Finally, the percentage of biofilm inhibition was calculated according to the formula described by [17]:

$$\text{Biofilm Inhibition (\%)} = \frac{\text{wavelength of control pit} - \text{wavelength of equation pit}}{\text{wavelength of the control pit}} \times 100$$

Effect of iron nanoparticles on the growth of pathogenic bacteria

The antibacterial activity of the synthesized iron nanoparticles (FeNPs) was investigated using the agar well diffusion method, as described by [18]. A stock solution was prepared by dissolving 0.001 g of iron nanoparticles, which was subsequently diluted to obtain final concentrations of 25, 50, 75, and 100 µg/mL.

The assay was performed against four distinct pathogenic bacterial species: *P. aeruginosa*, *E. coli*, *K. pneumoniae*, and *S. aureus*. Bacterial suspensions were uniformly inoculated onto Mueller-Hinton agar plates, and wells with a diameter of 6 mm were punctured into the agar surface using a sterile cork borer. A volume of 0.2 mL of each iron nanoparticle concentration was carefully introduced into its respective well. The plates were then incubated at 37 °C for 24 hours. After the incubation period, the antibacterial activity was evaluated by measuring the zone of inhibition diameters (in millimeters) around each well using a standard ruler, according to the method described by [19].

Results and discussion

The bacterial culture results indicated that out of 54 collected samples, 28 samples (51.9 %) showed positive growth, while 26 samples (48.1 %) showed negative growth. ***Table 1*** presents the bacterial species isolated in this study along with the number of isolates obtained for each species. As shown in the table, the distribution of the 28 isolates was as follows: *Pseudomonas aeruginosa* (8 isolates), *Escherichia coli* (7 isolates), *Klebsiella pneumoniae* (4 isolates), *Staphylococcus aureus* (4 isolates), *Bacillus cereus* (3 isolates), and *B. subtilis* (2 isolates).

The genus *Pseudomonas* is one of the most diverse bacterial groups, capable of thriving in a wide variety of environmental niches, including soil, water, plants, and animals. Unlike many other species within this genus, *P. aeruginosa* acts as a notable pathogen in animals [20]. The isolation rate of this species in the current study aligns with the findings of [21] and [22], who successfully isolated it from various soil types.

Table 1

Bacterial species isolated from soil samples and their frequency

No	Bacterial species	Frequency
1	*Pseudomonas aeruginosa*	8
2	*Escherichia coli*	7
3	*Klebsiella pneumoniae*	4
4	*Staphylococcus aureus*	4
5	*Bacillus cereus*	3
6	*Bacillus subtilis*	2

Similarly, *Klebsiella* species are ubiquitous in nature and frequently detected in soil, plants, sewage, surface water, and other environmental matrices. Among them, *K. pneumoniae* is a significant opportunistic pathogen belonging to the *Enterobacteriaceae* family, which is clinically associated with cutaneous, gastrointestinal, respiratory, and urinary tract infections [23, 24]. While some *K. pneumoniae* isolates are genuinely environmental strains flourishing in their natural habitat, others are likely introduced from human and animal sources, thus serving as environmental contaminants [25, 26]. In fact, soil, water, and vegetation have been well-established as natural habitats for *K. pneumoniae* [27]. Additionally, it has been demonstrated that clinical and environmental isolates of *K. pneumoniae* share highly similar phenotypic characteristics [28].

The bacterium *E. coli* is a facultative anaerobe. It is a mesophilic species that grows optimally between 37 °C and 42 °C; its growth is significantly hindered at lower temperatures and rapidly declines at higher temperatures. As a classic model organism, *E. coli* has been extensively researched to comprehend fundamental biological processes, including gene expression, replication, and metabolism. While the species contains numerous pathogenic strains, it is also widely utilized in biotechnology and medicine to produce recombinant proteins and enzymes [29]. Most research on *E. coli* in soils has been conducted through laboratory survival experiments using field-collected soil samples inoculated with specific bacterial strains. In these experiments, *E. coli* abundance (typically expressed as CFU/g) tends to decline quickly upon inoculation before leveling off until the bacterial levels fall below detection limits. According to previous reports, their lifespan in soil ranges from several weeks to months, or even up to 336 days; longer survival times have been observed in wetter soils and for commensal rather than pathogenic isolates [30].

Our *S. aureus* isolation results were consistent with [31], who demonstrated that certain soil characteristics significantly influence bacterial abundance, confirming that soils serve as a vital source of bacteria within watersheds. Understanding these sources is essential for implementing management measures aimed at reducing pathogen loads entering estuaries,

thereby minimizing transmission risks to recreational water users.

Furthermore, our study yielded the isolation of both *B. cereus* (3 isolates) and *B. subtilis* (2 isolates). These findings align with the results of [32], who reported that metal-contaminated soils can be effectively bioremediated by *Bacillus* species. When applied at controlled concentrations, these bacteria enhance carbon sequestration and function as powerful denitrifying agents in agroecosystems.

Numerous species and strains within the genus *Bacillus* are well-known for producing a wide array of antimicrobial compounds, including various antibiotics. Among them, *B. subtilis* is considered one of the most prominent producers, capable of synthesizing more than 70 distinct antibiotics. Some of its metabolites exhibit potent antifungal and antibacterial activities against several phytopathogenic microorganisms. Generally, *Bacillus* species are Gram-positive, rod-shaped, motile, and spore-forming bacteria commonly distributed across diverse environments, particularly in soil. Their remarkable ability to endure harsh environmental conditions is largely attributed to their capacity to generate resilient endospores through straightforward and rapid developmental cycles [33].

Microscopic Identification

Following the purification of the bacterial isolates, Gram staining revealed that the majority of the bacteria were Gram-negative rods, occurring either singly or in pairs, while some were Gram-positive, characterized by long and medium-sized rods arranged in chains. Additionally, certain bacterial samples appeared as Gram-positive spherical cells arranged in clusters.

The differentiation of the positive cultures indicated that Gram-negative bacteria constituted 64.3 % (18 isolates of the positive growth), whereas Gram-positive bacteria accounted for 35.7 % (10 isolates). Microscopic examination of *P. aeruginosa* showed Gram-negative, non-spore-forming rod cells, consistent with the observations of [34]. Under the microscope, *E. coli* appeared as single or paired non-spore-forming rods, as previously described by [35]. Microscopic examination of *K. pneumoniae* revealed short, Gram-negative rods [36]. In contrast, microscopic inspection of *B. subtilis* revealed Gram-positive rods arranged in short chains or pairs [37], while *B. cereus* displayed Gram-positive, rod-shaped cells appearing either single, paired, or in long chains [38]. Finally, microscopic examination and Gram staining of *S. aureus* demonstrated that the cells were spherical, Gram-positive, and clustered in characteristic grape-like formations, which serves as a key diagnostic feature to distinguish staphylococci [39].

Biosynthesis of iron nanoparticles (FeNPs)

The present study demonstrated that *Pseudomonas aeruginosa* possesses the capability to biosynthesize iron nanoparticles. The physicochemical properties of the synthesized nanoparticles were systematically confirmed using the following characterization techniques:

Visual observation (color variation)

The primary macro-morphological indication of successful nanoparticle biosynthesis is a distinct color variation of the reaction mixture. ***Figure 1*** shows the color variation of iron nanoparticles produced by Pseudomonas aeruginosa. The current results align with the findings reported by [7], where the color of the solution transitionally changed from yellow to a dark brown hue, confirming the reduction of iron ions and the formation of FeNPs.

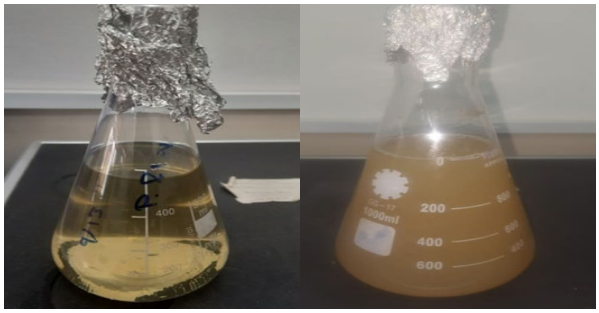

A B

Figure 1. Color variation of iron nanoparticles produced by Pseudomonas aeruginosa:
A – initial cell-free culture supernatant before the reaction, and
B – synthesized nanoparticle solution after the addition of iron nitrate

UV-visible spectroscopy

The next step in verifying nanoparticle synthesis involves measuring the optical absorbance spectrum, as each nanomaterial exhibits a characteristic absorption profile. ***Figure 2*** shows the UV-visible spectrum of FeNPs produced by *Pseudomonas aeruginosa*. The scanning wavelength for the synthesized iron nanoparticles ranged from 200 to 700 nm. The characteristic surface plasmon resonance (SPR) absorption peak of the iron nanoparticles was observed at a wavelength of 304 nm. The spectrophotometric profiles obtained in this study align with the results previously reported by [40].

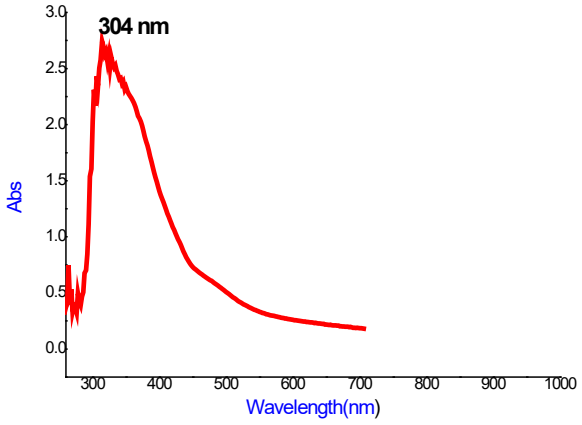

Figure 2. UV-visible absorbance spectrum of FeNPs produced by *Pseudomonas aeruginosa*

Fourier-transform infrared (FT-IR) spectroscopy

The functional surface groups present in the biosynthesized iron nanoparticles were identified using FT-IR spectroscopy. The resulting vibrational frequencies and absorption bands were interpreted using the analytical tools available on the InstaNANO platform, which facilitates the

rapid identification of active biomolecules, chemical compounds, and specific functional groups based on their peak values. ***Table 2*** and ***Figure 3*** present the characteristic FT-IR absorption peaks and the respective types of active functional groups involved in the capping, stabilization, and green synthesis of the nanoparticles.

Table 2

FT-IR peak assignments and functional groups of FeNPs synthesized by *Pseudomonas aeruginosa*

Peak (cm^{-1})	Functional group / Vibrational mode	Compound class
3833.79	O–H stretching	Alcohols / Phenols
3741.23	O–H / N–H stretching	Alcohols / Amides
3617.80	O–H stretching (free)	Alcohols / Phenols
3274.54	N–H stretching / O–H bonded	Alcohols / Amines
2919.70	C–H stretching	Alkanes
2360.44	O=C=O stretching (CO_2) background) / N–H stretching	Amine salts / Ambient atmosphere
1643.05	C=C stretching / C=N stretching	Alkenes / Imines / Oximes
960.38	C–H bending / O–H bending	Alkenes / Carboxylic acids
589.97	Fe–O stretching / C–X stretching	Metal oxides / Halo compounds

The FT-IR spectroscopic analysis verified the presence of various functional groups capping the surface of the biosynthesized iron nanoparticles (***Table 2***). The absorption bands observed in the higher frequency region, particularly around 3833.79–3274.54 cm^{-1}, correspond to the stretching vibrations of hydroxyl (O–H) and amine/amide (N–H) groups, which are characteristic of bacterial proteins and carbohydrates. The distinct peak at 1643.05 cm^{-1} is attributed to the C=C or C=N stretching modes, suggesting the involvement of microbial metabolites in the stabilizing processes. Crucially, the lower frequency band at 589.97 cm^{-1} confirms the successful formation of the metal-oxygen (Fe–O) bond, establishing the definitive chemical synthesis of iron oxide nanoparticles by *P. aeruginosa*.

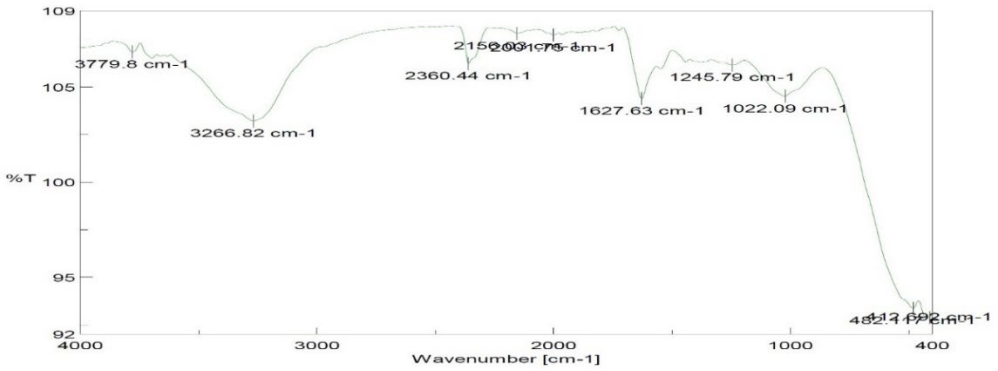

Figure 3. FT-IR spectrum of the synthesized iron nanoparticles (FeNPs) displaying key functional groups and their corresponding absorption bands

Scanning electron microscopy (SEM) analysis

The shape, size distribution, and surface morphology of the synthesized nanoparticles were evaluated using scanning electron microscopy (SEM). The electron micrographs of the iron nanoparticles revealed a variety of morphologies; however, a spherical shape was predominantly observed. The particle sizes were found to range around a representative value of D_1 = 22.83 nm, as shown in ***Figure 4***.

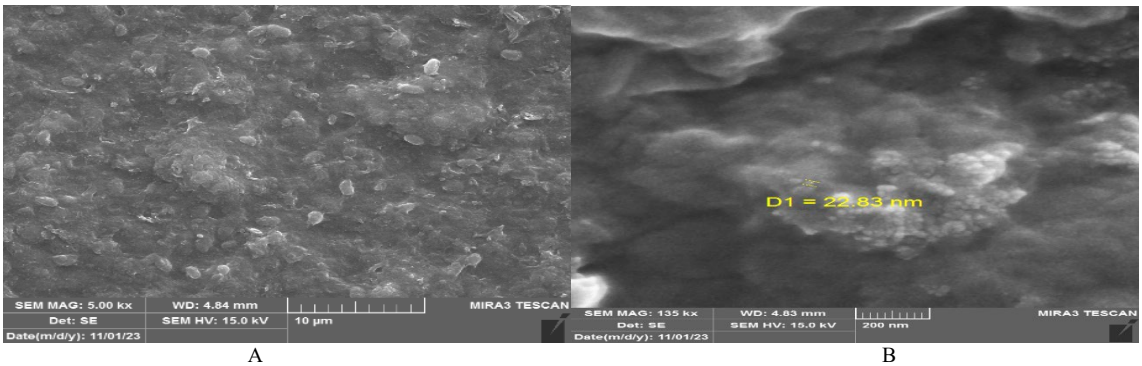

A B

Figure 4. SEM micrographs of the biosynthesized iron nanoparticles (FeNPs) produced by *Pseudomonas aeruginosa*: A – low-magnification view showing surface topography and particle agglomeration, and B – high-magnification view demonstrating a representative spherical nanoparticle with a measured individual diameter of D_1 = 22.83 nm

The SEM images demonstrated that the nanoparticles possess a smooth surface topography with a relatively uniform spherical shell structure. The observed enlargement or agglomeration of certain smaller particles might be attributed to the high thermal conditions during processing. At lower temperatures, the precursor units tend to establish stronger cohesive bonds, which subsequently drives the assembly into well-defined spherical shell formations. The morphological findings obtained in this current study align with the results previously reported by [7].

Molecular Identification

Molecular identification of the bacterial isolates was carried out using the polymerase chain reaction (PCR) targeting the 16S rRNA gene, a highly conserved genetic marker commonly utilized in bacterial taxonomy and phylogenetic analysis [41]. Following genomic DNA extraction, agarose gel electrophoresis confirmed the presence of intact genomic DNA, as evidenced by clear and distinct bands.

The 16S rRNA gene was successfully amplified using specific primers, and the resulting PCR products were analyzed via agarose gel electrophoresis and compared against a DNA ladder (molecular weight marker). As shown in ***Figure 5***, the results revealed a distinct band at approximately 1400 base pairs (bp), which is highly consistent with the expected size of the 16S rRNA gene fragment. These molecular findings align with the results reported in previous studies [42, 43].

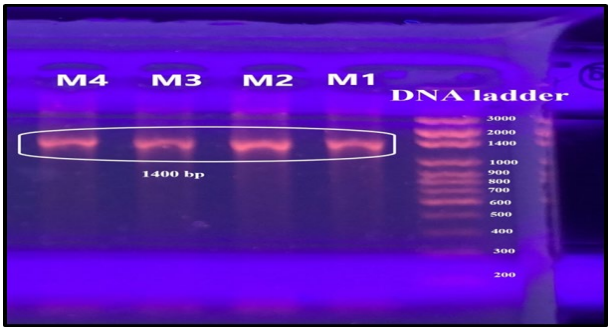

Figure 5. Agarose gel electrophoresis (1 %) showing PCR amplification products of the bacterial 16S rRNA gene. Lane DNA ladder: 200–3000 bp molecular weight marker; Lanes M1, M2, M3, and M4: positive bacterial isolates displaying the expected amplicon product length of approximately 1400 bp

The success of the genomic amplification was visually confirmed via agarose gel electrophoresis (***Figure 5***). As illustrated, all four analyzed bacterial isolates (Lanes M1–M4) exhibited a single, sharp, and highly intense band. The migration distance of these PCR products, when compared against the 3000 bp DNA ladder, corresponded precisely to the expected molecular weight of approximately 1400 bp. The absence of non-specific amplification or primer-dimer bands indicates the high specificity of the utilized primers and the purity of the extracted template DNA, definitively confirming the taxonomic suitability of the isolates for further 16S rRNA sequencing.

Screening of biofilm-forming bacteria via Congo Red Agar assay

The four pathogenic bacterial isolates (*P. aeruginosa*, *E. coli*, *K. pneumoniae*, and *S. aureus*) were cultured on Congo red agar (CRA) medium to evaluate their phenotypic capacity for biofilm formation. This screening method relies on the specific chemical interaction between the exopolysaccharide (EPS) components of the extracellular biofilm matrix and the Congo red dye. The development of distinct black colonies indicates robust, strong biofilm production. Furthermore, the intensity of this black coloration directly reflects a high level of extracellular polysaccharide synthesis and matrix secretion, as systematically illustrated in ***Figure 6***.

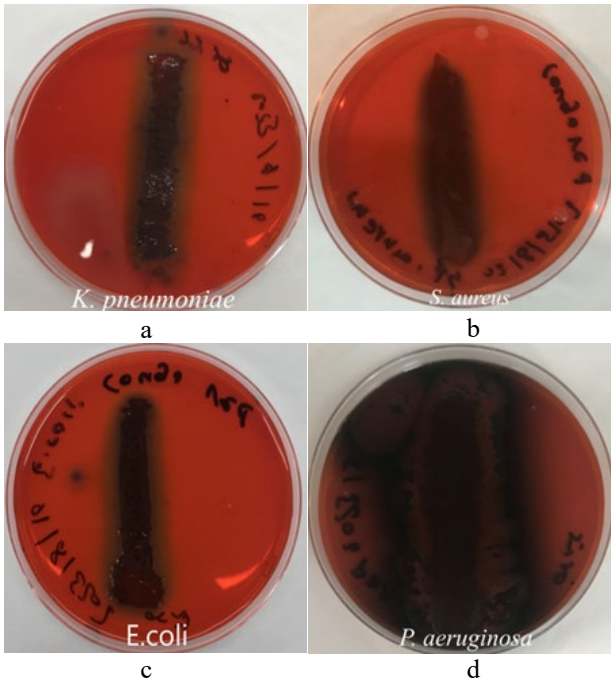

Figure 6. Phenotypic screening of biofilm-forming bacteria on Congo red agar (CRA) medium, demonstrating characteristic black colonies due to robust exopolysaccharide production in:
a – *Klebsiella pneumoniae*, b – *Staphylococcus aureus*, c – *Escherichia coli*, and d – *Pseudomonas aeruginosa*

The phenotypic screening on Congo red agar (CRA) plates confirmed that all four examined pathogenic isolates possess robust biofilm-forming capabilities (***Figure 6***). *P. aeruginosa* (***Figure 6d***) exhibited the most intense, deep black coloration with a dry, crystalline colony morphology, indicating an exceptionally high rate of exopolysaccharide (EPS) secretion. This was closely followed by *K. pneumoniae* (***Figure 6a***) and *E. coli* (***Figure 6c***), both of which developed distinct, dark black streaks due to active interaction with the Congo red dye. The Gram-positive pathogen *S. aureus* (***Figure 6b***) also formed prominent dark brownish-black colonies, confirming its ability to synthesize extracellular matrix components. These qualitative macroscopic observations demonstrate that all four strains are active biofilm producers, establishing a solid baseline for subsequent quantitative evaluations and nanoparticle treatment assays.

Quantitative determination of biofilm formation via Microtiter Plate (MTP) assay

The quantitative evaluation of biofilm formation by the four pathogenic bacterial isolates was performed using the microtiter plate (MTP) assay. The spectrophotometric results demonstrated that all four isolates possessed a strong capacity to produce high-density biofilms, as summarized in ***Table 3***. All tested strains significantly exceeded the threshold for strong biofilm production ($A > 2 \times A_C$).

Table 3
Quantitative classification of biofilm formation by the pathogenic isolates using the Microtiter Plate (MTP) assay

Bacterial species	Control absorbance (A_C)	Isolate absorbance (A)	Mathematical condition	Biofilm intensity
Pseudomonas aeruginosa	0.098	1.136	1.136 > 2 × 0.098	Strong
Escherichia coli	0.075	1.513	1.513 > 2 × 0.075	Strong
Klebsiella pneumoniae	0.097	1.165	1.165 > 2 × 0.097	Strong
Staphylococcus aureus	0.108	1.329	1.329 > 2 × 0.108	Strong

The quantitative spectrophotometric data confirmed a highly significant shift in optical density values compared to the negative controls ***(Table 3***). All four tested pathogens demonstrated an outstanding capacity for architectural cell attachment, with absorbance values (A) exceeding the strict threshold for strong biofilm production by up to 10-fold to 20-fold. Notably, Escherichia coli exhibited the highest optical accumulation value (A = 1.513), followed closely by Staphylococcus aureus (A = 1.329). These quantitative results strongly support current global microbiologic reports highlighting the clinical persistence of these high-priority strains due to their stable extracellular polymeric matrices. The robust baseline formation rates observed across both Gram-negative and Gram-positive isolates underscore the urgent need for innovative non-antibiotic intervention strategies, such as target-delivered nanomaterials and bio-inspired metallic complexes.

Evaluation of biofilm inhibition by synthesized iron nanoparticles (FeNPs)

The current study demonstrated a robust, concentration-dependent inhibitory effect of the biosynthesized iron nanoparticles (FeNPs) against the biofilm-forming bacterial isolates. As summarized in ***Table 4***, the highest biofilm inhibition rate was achieved against *S. aureus*, reaching 91.64 % at a nanoparticle concentration of 100 µg/mL, while the lowest inhibition for the same pathogen was 89.69 % at 50 µg/mL. Similar concentration-dependent trends were recorded for *P. aeruginosa* (91.48 % at 100 µg/mL and 90.19 % at 50 µg/mL), *E. coli* (91.61 % at 100 µg/mL and 90.21 % at 50 µg/mL), and *K. pneumoniae* (91.22 % at 100 µg/mL and 89.91 % at 50 µg/mL).

Table 4
Biofilm inhibition rates (%) of pathogenic bacterial isolates treated with different concentrations of biosynthesized FeNPs

Bacterial species	100 µg/mL	50 µg/mL
Pseudomonas aeruginosa	91.48 %	90.19 %
Escherichia coli	91.61 %	90.21 %
Klebsiella pneumoniae	91.22 %	89.91 %
Staphylococcus aureus	91.64 %	89.69 %

The observed variations in biofilm inhibition among these pathogenic species may be attributed to distinct differences in cell wall structures, extracellular polymeric substance (EPS) composition, and individual susceptibility to nanoparticle interactions [44]. Oxidative stress induced by metal oxides is widely recognized as the primary mechanism underlying the antimicrobial and antibiofilm activities of iron oxide nanoparticles. These FeNPs typically carry a net positive surface charge, whereas the surfaces of bacterial cells are net-negatively charged. This electrostatic attraction significantly enhances the adhesion of the nanoparticles to the bacterial cell envelope, subsequently promoting cell membrane rupture, the localized generation of reactive oxygen species (ROS), irreversible damage to intracellular components, and ultimately, bacterial cell death [45].

Antimicrobial activity of biosynthesized iron nanoparticles (FeNPs)

The biosynthesized iron nanoparticles (FeNPs) demonstrated distinct, dose-dependent antibacterial activity against all tested pathogenic isolates, with the diameters of the inhibition zones increasing proportionally with nanoparticle concentration (***Table 5***). Representative agar plates illustrating this concentration-dependent expansion of the inhibition zones (at 25, 50, 75, and 100 µg/mL) across the four pathogenic strains are presented in ***Figure 7a–d***, respectively. The most potent inhibitory effect was observed against *P. aeruginosa*, where the zone of inhibition reached a maximum of 21 mm at a concentration of 100 µg/mL. Conversely, *E. coli* exhibited the lowest sensitivity, with a minimum inhibition zone of 12 mm recorded at a concentration of 25 µg/mL.

Table 5
Zones of inhibition (mm) of biosynthesized FeNPs against the tested pathogenic bacteria

Pathogenic bacteria	25 µg/mL	50 µg/mL	75 µg/mL	100 µg/mL
Pseudomonas aeruginosa	14.5	15.5	19.6	21.0
Escherichia coli	12.0	12.7	14.0	14.5
Klebsiella pneumoniae	13.2	14.5	15.6	17.0
Staphylococcus aureus	14.0	15.0	15.0	16.0

A clear concentration-dependent expansion of the inhibition zones was evident across all tested isolates. For *P. aeruginosa*, the zones of inhibition increased from 14.5 mm (at 25 µg/mL) to 21 mm (at 100 µg/mL), representing an increase of approximately 44.8 %. *K. pneumoniae* demonstrated a 28.3 % increase (from 13.25 mm to 17 mm), while *E. coli* recorded a relative increase of 20.8 % (from 12 mm to 14.5 mm). *S. aureus*

exhibited the smallest relative increase of 14.3 %, with zones expanding from 14 mm to 16 mm.

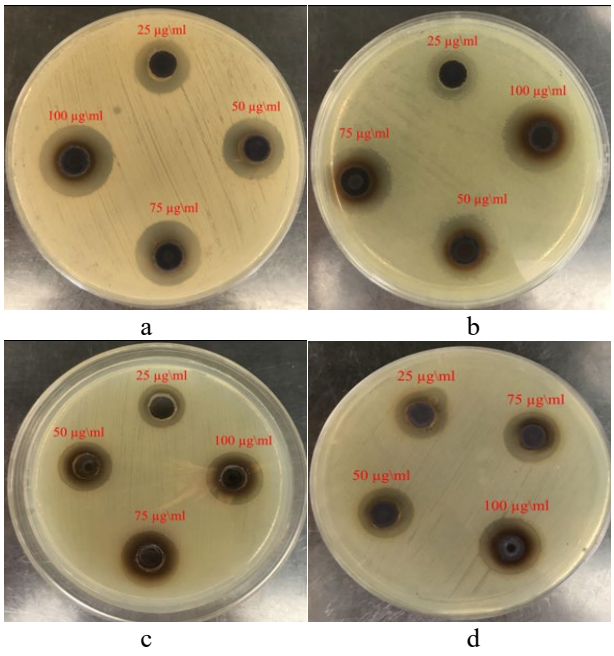

Figure 7. Zones of inhibition demonstrating the concentration-dependent antibacterial activity of FeNPs against the tested pathogenic bacteria in: a – *Klebsiella pneumoniae*, b – *Staphylococcus aureus*, c – *Escherichia coli*, and d – *Pseudomonas aeruginosa*

Variations in susceptibility among the bacterial isolates may be attributed to distinct differences in cell wall architecture, membrane permeability, metabolic activity, and unique genetic determinants that influence cellular stress-response mechanisms, as discussed by [46]. Specifically, Gram-negative bacteria possess an outer lipopolysaccharide membrane that can strictly modulate nanoparticle penetration, whereas Gram-positive bacteria lack this outer membrane but feature a significantly thicker, highly cross-linked peptidoglycan layer that directly influences nanoparticle interaction dynamics [47]. Furthermore, FeNP-induced antibacterial activity is deeply linked to metal-driven oxidative stress mechanisms, cell envelope disruption, and subsequent interference with essential intracellular enzymatic pathways [48].

Statistical analysis was performed by presenting the quantitative data as mean ± standard deviation (SD) derived from three independent replicates. A one-way analysis of variance (ANOVA) was subsequently applied to compare the inhibition zones across the different concentrations for each bacterial species, followed by Tukey's Honestly Significant Difference (HSD) post-hoc test to evaluate pairwise differences between specific concentrations. Based on the concentration-dependent trends, the antibacterial inhibition achieved at 75 and 100 µg/mL was significantly greater ($p<0.05$) than that observed at 25 µg/mL. Furthermore, interspecies comparisons at the 100 µg/mL concentration revealed statistically significant differences, particularly between the highly susceptible *P. aeruginosa* and the less sensitive *E. coli*.

Conclusions

This study documented the successful green synthesis of iron nanoparticles (FeNPs) using *Pseudomonas aeruginosa* isolated from soil samples. The successful formation and optical properties of the biogenic FeNPs were confirmed by UV-visible spectroscopy with a distinct absorption peak at 304 nm, while FT-IR analysis definitively verified the presence of the characteristic metal-oxygen (Fe–O) bond at 589.97 cm^{-1} along with stabilizing bacterial biomolecules. Scanning electron microscopy (SEM) confirmed a predominantly spherical morphology with a representative particle diameter of 22.83 nm.

The biosynthesized nanoparticles demonstrated exceptional concentration-dependent antibacterial and antibiofilm activities against high-priority pathogens (*P. aeruginosa*, *E. coli*, *K. pneumoniae*, and *S. aureus*). The quantitative microtiter plate assay revealed robust antibiofilm efficacy, reaching a maximum eradication rate of 91.64 % against *S. aureus* at 100 µg/mL. Furthermore, the agar well diffusion test demonstrated substantial growth inhibition zones of up to 21.0 mm against *P. aeruginosa*. Taken together, these definitive findings indicate the high potential of biosynthesized iron nanoparticles to serve as highly effective, biocompatible, and environmentally friendly nano-antimicrobials for controlling multi-drug resistant pathogens and mitigating persistent biofilm-associated infections.

DECLARATIONS

Ethical Statement

The authors declare that this study did not involve any human participants, clinical specimens, or vertebrate animal subjects. All experimental procedures were conducted strictly using bacterial strains isolated from environmental soil samples. Therefore, formal institutional ethical review and approval were not required for this investigation.

Funding

This research received no external funding.

Conflict of Interest

The author declares no conflict of interest.

Acknowledgements

None.

Declaration of AI and AI-assisted technologies

The author declares that no artificial intelligence or AI-assisted technologies were used in the preparation of this manuscript.

References

1. Jin, S. (2024). Pseudomonas aeruginosa. In Y.-W. Tang, M. Sussman, D. Liu, I. Poxton, & J. Schwartzman (Eds.), *Molecular medical microbiology* (3rd ed., pp. 811–825). Academic Press. https://doi.org/10.1016/B978-0-12-818619-0.00064-2
2. Kuraimsh, K. K. (2025). Prevalence of resistance to antimicrobial agents by Pseudomonas aeruginosa and Acinetobacter baumannii isolated from Iraqi patients with burns at Al-Nasiriya Hospital. *Journal of the Faculty of Medicine Baghdad*, 67 (4), 447–456. https://doi.org/10.32007/jfacmedbaghdad3204

3. Khan, F., Jeong, G.-J., Singh, P., Tabassum, N., Mijakovic, I., & Kim, Y.-M. (2022). Retrospective analysis of the key molecules involved in the green synthesis of nanoparticles. *Nanoscale*, 14 (40), 14824–14857. https://doi.org/10.1039/d2nr03632k
4. Dutt, Y., Pandey, R. P., Dutt, M., Gupta, A., Vibhuti, A., Vidic, J., Raj, V. S., Chang, C.-M., & Priyadarshini, A. (2023). Therapeutic applications of nanobiotechnology. *Journal of Nanobiotechnology*, 21 (1). https://doi.org/10.1186/s12951-023-01909-z
5. Tabassum, N., Khan, F., Kang, M.-G., Jo, D.-M., Cho, K.-J., & Kim, Y.-M. (2023). Inhibition of polymicrobial biofilms of *Candida albicans – Staphylococcus aureus*/*Streptococcus mutans* by fucoidan–gold nanoparticles. *Marine Drugs*, 21 (2), 123. https://doi.org/10.3390/md21020123
6. Singh, P., Pandit, S., Beshay, M., Mokkapati, V. R. S. S., Garnaes, J., Olsson, M. E., Sultan, A., Mackevica, A., Mateiu, R. V., Lütken, H., Daugaard, A. E., Baun, A., & Mijakovic, I. (2018). Anti-biofilm effects of gold and silver nanoparticles synthesized by the *Rhodiola rosea* rhizome extracts. *Artificial Cells, Nanomedicine, and Biotechnology*, 46 (sup3), 886–899. https://doi.org/10.1080/21691401.2018.1518909
7. Khan, A. A., Khan, S., Khan, S., Rentschler, S., Laufer, S., & Deigner, H.-P. (2021). Biosynthesis of iron oxide magnetic nanoparticles using clinically isolated *Pseudomonas aeruginosa*. *Scientific Reports*, 11 (1). https://doi.org/10.1038/s41598-021-99814-8
8. Asoso, O. S., Idris, O. O., Ayodele, O. S., & Laoye, B. J. (2022). Isolation and identification of bacteria and fungi associated with tomatoes. *Medical & Clinical Research*, 7 (6), 1–11. https://doi.org/10.33140/mcr.07.06.02
9. Sambrook, J., & Russell, D. W. (2006). Purification of nucleic acids by extraction with phenol: Chloroform. *Cold Spring Harbor Protocols*, 2006 (1), pdb. https://doi.org/10.1101/pdb.prot4455
10. Leszczewicz, M., Broncel, N., Frączak, O., Kapela, T., & Makowski, K. (2025). Screening of moderately halophilic bacteria producing ectoine resulting in selection of *Virgibacillus salarius* BHTA19. *Food Technology and Biotechnology*, 63 (3), 310. https://doi.org/10.17113/ftb.63.03.25.8727
11. Shenoy, V., Harika, K., Narasimhaswamy, N., & Chawla, K. (2020). Detection of biofilm production and its impact on antibiotic resistance profile of bacterial isolates from chronic wound infections. *Journal of Global Infectious Diseases*, 12 (3), 129–134. https://doi.org/10.4103/jgid.jgid_150_19
12. Almeida, C., Azevedo, N. F., Santos, S., Keevil, C. W., & Vieira, M. J. (2011). Discriminating multi-species populations in biofilms with peptide nucleic acid fluorescence *in situ* hybridization (PNA FISH). *PLoS ONE*, 6 (3), e14786. https://doi.org/10.1371/journal.pone.0014786
13. Tang, J., Kang, M., Chen, H., Shi, X., Zhou, R., Chen, J., & Du, Y. (2011). The staphylococcal nuclease prevents biofilm formation in *Staphylococcus aureus* and other biofilm-forming bacteria. *Science China Life Sciences*, 54 (9), 863–869. https://doi.org/10.1007/s11427-011-4195-5
14. Kamnev, A. A., Dyatlova, Y. A., Kenzhegulov, O. A., Vladimirova, A. A., Mamchenkova, P. V., & Tugarova, A. V. (2021). Fourier Transform Infrared (FTIR) spectroscopic analyses of microbiological samples and biogenic selenium nanoparticles of microbial origin: Sample preparation effects. *Molecules*, 26 (4), 1146. https://doi.org/10.3390/molecules26041146
15. Ashrafi-Saiedlou, S., Rasouli-Sadaghiani, M., Fattahi, M., & Ghosta, Y. (2025). Biosynthesis and characterization of iron oxide nanoparticles fabricated using cell-free supernatant of Pseudomonas fluorescens for antibacterial, antifungal, antioxidant, and photocatalytic applications. *Scientific Reports*, 15 (1). https://doi.org/10.1038/s41598-024-84974-0
16. Mathur, T., Singhal, S., Khan, S., Upadhyay, D., Fatma, T., & Rattan, A. (2006). Detection of biofilm formation among the clinical isolates of Staphylococci: An evaluation of three different screening methods. *Indian Journal of Medical Microbiology*, 24 (1), 25. https://doi.org/10.4103/0255-0857.19890
17. Majumdar, M., Khan, S. A., Nandi, N. B., Roy, S., Panja, A. S., Roy, D. N., & Misra, T. K. (2020). Green synthesis of iron nanoparticles for investigation of biofilm inhibition property. *ChemistrySelect*, 5 (43), 13575–13583. https://doi.org/10.1002/slct.202003033
18. Kamble, S., Bhosale, K., Mohite, M., & Navale, S. (2023). Methods of preparation of nanoparticles. *International Journal of Advanced Research in Science, Communication and Technology*, 3 (7), 121–126. https://doi.org/10.48175/IJARSCT-9485
19. Huseen, R., Taha, A., & Abdulhusein, O. (2021). Study of biological activities of magnetic iron oxide nanoparticles prepared by co-precipitation method. *Journal of Applied Sciences and Nanotechnology*, 1 (2), 37–48. https://doi.org/10.53293/jasn.2021.11635
20. Aghamollaei, H., Moghaddam, M. M., Kooshki, H., Heiat, M., Mirnejad, R., & Barzi, N. S. (2015). Detection of *Pseudomonas aeruginosa* by a triplex polymerase chain reaction assay based on lasI/R and gyrB genes. *Journal of Infection and Public Health*, 8 (4), 314–322. https://doi.org/10.1016/j.jiph.2015.03.003
21. Kridi, N., Al-Shater, M. S., & Al Zoubi, M. M. (2021). Isolation and identification of some bacterial isolates from soil contaminated with crude oil and Testing Their Effectiveness. *Baghdad Science Journal*, 18 (4). https://doi.org/10.21123/bsj.2021.18.4(suppl.).1476
22. Ali, A. A., Hameed, K. W., & Nadder, M. I. (2022). Isolation of Pseudomonas aeruginosa from soil and production of lipase enzyme. *IOP Conference Series: Earth and Environmental Science*, 961 (1), 012087. https://doi.org/10.1088/1755-1315/961/1/012087
23. Podschun, R., & Ullmann, U. (1998). *Klebsiella* spp. as nosocomial pathogens: Epidemiology, taxonomy, typing methods, and pathogenicity factors. *Clinical Microbiology Reviews*, 11 (4), 589–603. https://doi.org/10.1128/cmr.11.4.589
24. Wyres, K. L., & Holt, K. E. (2016). *Klebsiella pneumoniae* population genomics and antimicrobial-resistant clones. *Trends in Microbiology*, 24 (12), 944–956. https://doi.org/10.1016/j.tim.2016.09.007
25. Yang, F., Deng, B., Liao, W., Wang, P., Chen, P., & Wei, J. (2019). High rate of multiresistant *Klebsiella pneumoniae* from human and animal origin. *Infection and Drug Resistance*, 12, 2729–2737. https://doi.org/10.2147/idr.s219155
26. Chi, X., Berglund, B., Zou, H., Zheng, B., Börjesson, S., Ji, X., Ottoson, J., Lundborg, C. S., Li, X., & Nilsson, L. E. (2019). Characterization of clinically relevant strains of extended-spectrum β-lactamase-producing *Klebsiella pneumoniae* occurring in environmental sources in a rural area of China by using whole-genome sequencing. *Frontiers in Microbiology*, 10, 211. https://doi.org/10.3389/fmicb.2019.00211
27. Kämpfer, P., & Glaeser, S. P. (2013). Prokaryote characterization and identification. In E. Rosenberg, E. F. DeLong, S. Lory, E. Stackebrandt, & F. Thompson (Eds.), *The Prokaryotes: Prokaryotic biology and symbiotic associations* (4th ed., pp. 123–147). Springer. https://doi.org/10.1007/978-3-642-30194-0_6
28. Rocha, J., Henriques, I., Gomila, M., & Manaia, C. M. (2022). Common and distinctive genomic features of *Klebsiella pneumoniae* thriving in the natural environment or in clinical settings. *Scientific Reports*, 12 (1). https://doi.org/10.1038/s41598-022-14547-6
29. Verheijen, F., Jelinčić, A., Jeffery, S., Domingos, T., Khodaparast, Z., & Bastos, A. C. (2025). Correction: *Escherichia coli* thrives in soil 24 months after grazing exclusion in a rainfed Mediterranean biodiverse pasture. *Frontiers in Environmental Science*, 13. https://doi.org/10.3389/fenvs.2025.1708183
30. Murphy, C. M., Weller, D. L., Bardsley, C. A., Ingram, D. T., Chen, Y., Oryang, D., Rideout, S. L., & Strawn, L. K. (2024). Survival of twelve pathogenic and generic *Escherichia coli* strains in agricultural soils as influenced by strain, soil type, irrigation regimen, and soil amendment. *Journal of Food Protection*, 87 (10), 100343. https://doi.org/10.1016/j.jfp.2024.100343
31. Gerken, T., Wiegner, T. N., & Economy, L. M. (2022). A comparison of soil *Staphylococcus aureus* and fecal indicator bacteria concentrations across land uses in a Hawaiian watershed. *Journal of Environmental Quality*, 51 (5), 916–929. https://doi.org/10.1002/jeq2.20380
32. Mahapatra, S., Yadav, R., & Ramakrishna, W. (2022). *Bacillus subtilis* impact on plant growth, soil health and environment: Dr. Jekyll and Mr. Hyde. *Journal of Applied Microbiology*, 132 (5), 3543–3562. https://doi.org/10.1111/jam.15480
33. Foysal, M. J., & Lisa, A. K. (2018). Isolation and characterization of *Bacillus* sp. strain BC01 from soil displaying potent antagonistic activity against plant and fish pathogenic fungi and bacteria. *Journal of Genetic Engineering and Biotechnology*, 16 (2), 387–392. https://doi.org/10.1016/j.jgeb.2018.01.005

34. Al-Mojamaee, N. A. H., & Altaii, H. A. J. (2023). Comparison of two methods for the detection of *Pseudomonas aeruginosa* biofilm formation isolated from different clinical samples. *Iraqi Journal of Humanities and Social Science Research*, 11 (3), 651–668.
35. Basavaraju, M., & Gunashree, B. S. (2022). *Escherichia coli*: An overview of main characteristics. In M. S. Erjavec (Ed.), *Escherichia coli: Old and new insights* (pp. 1–18). IntechOpen. https://doi.org/10.5772/intechopen.105508
36. Abbas, R., Chakkour, M., Zein El Dine, H., Obaseki, E. F., Obeid, S. T., Jezzini, A., Ghssein, G., & Ezzeddine, Z. (2024). General overview of *Klebsiella pneumoniae*: Epidemiology and the role of siderophores in its pathogenicity. *Biology*, 13 (2), 78. https://doi.org/10.3390/biology13020078
37. Todorova, S., & Kozhuharova, L. (2009). Characteristics and antimicrobial activity of *Bacillus subtilis* strains isolated from soil. *World Journal of Microbiology and Biotechnology*, 26 (7), 1207–1216. https://doi.org/10.1007/s11274-009-0290-1
38. Stecchini, M. L., Spaziani, M., Torre, M. D., & Pacor, S. (2009). *Bacillus cereus* cell and spore properties as influenced by the micro-structure of the medium. *Journal of Applied Microbiology*, 106 (6), 1838–1848. https://doi.org/10.1111/j.1365-2672.2009.04162.x
39. Silva-Santana, G., Cabral-Oliveira, G. G., Oliveira, D. R., Nogueira, B. A., Pereira-Ribeiro, P. M. A., & Mattos-Guaraldi, A. L. (2020). *Staphylococcus aureus* biofilms: an opportunistic pathogen with multidrug resistance. *Reviews in Medical Microbiology*, 32 (1), 12–21. https://doi.org/10.1097/mrm.0000000000000223
40. Hajiali, S., Daneshjou, S., & Daneshjoo, S. (2022). Biomimetic synthesis of iron oxide nanoparticles from *Bacillus megaterium* to be used in hyperthermia therapy. *AMB Express*, 12 (1). https://doi.org/10.1186/s13568-022-01490-y
41. Qurban, A., & Ameen, A. (2020). Bacterial identification by 16S ribotyping: A review. *Biotechnology: An Indian Journal*, 16 (2), 204.
42. Prashanthi, R., Shreevatsa, G. K., Krupalini, S., & Manoj, L. (2021). Isolation, characterization, and molecular identification of soil bacteria showing antibacterial activity against human pathogenic bacteria. *Journal of Genetic Engineering and Biotechnology*, 19 (1), 120. https://doi.org/10.1186/s43141-021-00219-x
43. Al-Dhabaan, F. A. (2019). Morphological, biochemical and molecular identification of petroleum hydrocarbons biodegradation bacteria isolated from oil polluted soil in Dhahran, Saud Arabia. *Saudi Journal of Biological Sciences*, 26 (6), 1247–1252. https://doi.org/10.1016/j.sjbs.2018.05.029
44. Singh, B., Dahiya, M., Kumar, V., Ayyagari, A., Chaudhari, D. N., & Ahire, J. J. (2025). Biofilm and antimicrobial resistance: Mechanisms, implications, and emerging solutions. *Microbiology Research*, 16 (8), 183. https://doi.org/10.3390/microbiolres16080183
45. Shkodenko, L., Kassirov, I., & Koshel, E. (2020). Metal oxide nanoparticles against bacterial biofilms: Perspectives and limitations. *Microorganisms*, 8 (10), 1545. https://doi.org/10.3390/microorganisms8101545
46. Dawan, J., & Ahn, J. (2022). Bacterial stress responses as potential targets in overcoming antibiotic resistance. *Microorganisms*, 10 (7), 1385. https://doi.org/10.3390/microorganisms10071385
47. Carnero Canales, C. S., Marquez Cazorla, J. I., Marquez Cazorla, R. M., Sábio, R. M., Santos, H. A., & Pavan, F. R. (2025). Combating Gram-negative infections: The role of antimicrobial peptides and nanotechnology in overcoming antibiotic resistance. *Materials Today Bio*, 35, 102381. https://doi.org/10.1016/j.mtbio.2025.102381
48. Zhang, T.-G., & Miao, C.-Y. (2024). Iron oxide nanoparticles as promising antibacterial agents of new generation. *Nanomaterials*, 14 (15), 1311. https://doi.org/10.3390/nano14151311

ORCID

I. J. Abbass https://orcid.org/0000-0003-0791-6778
E. A. Al-Imara https://orcid.org/0000-0002-7765-8332
D. A. Alhasan https://orcid.org/0000-0002-6992-5525